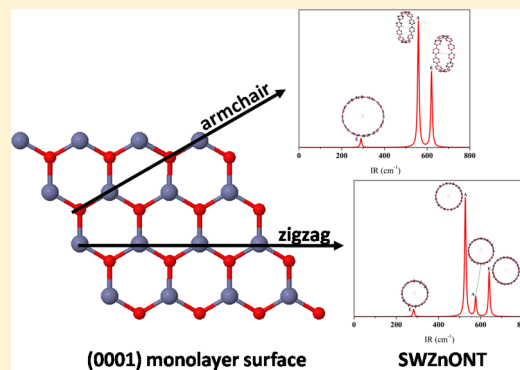


# Structural, Electronic, Vibrational, and Topological Analysis of Single-Walled Zinc Oxide Nanotubes

Naiara L. Marana,<sup>†</sup> Silvia Casassa,<sup>‡</sup> Elson Longo,<sup>§</sup> and Julio R. Sambrano<sup>\*,†</sup><sup>†</sup>Modeling and Molecular Simulations Group, São Paulo State University, UNESP, 17033-360, Bauru, SP, Brazil<sup>‡</sup>Theoretical Group of Chemistry, Chemistry Department, Torino University, Torino, Italy<sup>§</sup>Chemistry Institute, São Paulo State University, UNESP, 14801-907 Araraquara, SP, Brazil

## Supporting Information

**ABSTRACT:** Single-walled armchair and zigzag ZnO nanotubes (SWZnONTs) have been studied via periodic computational simulations based on density functional theory with the B3LYP, HSE06, PBE0, and PWGGA functional and all-electron basis set. The influence of the diameter of the nanotubes was carried out with respect to the bond length (Zn–O), bond angles (Zn–O–Zn), energy strain, band gap, density of states (DOS), band structures, vibrational analysis, and topological analysis of the electron density according to the quantum theory of atoms in molecules applied to the solid state. Its nanotubes properties were compared with the ZnO bulk and (0001) monolayer surface. The topological analysis, infrared and Raman spectra, and its vibrational modes at increasing diameter are reported for the first time. Owing to these analysis, both chiralities with large diameter can be used interchangeably in semiconductor applications. These theoretical models can be extended to study further issues, such as the effects caused by the addition of dopant and the interaction of molecules inside and/or outside of the nanotube.



## INTRODUCTION

Owing to its electronic and electro-optical properties, zinc oxide (ZnO) is widely used in technological applications. The direct wide band gap energy (3.37 eV) and large excitation binding energy (60 meV) enable its application in diodes, transistors, and energy conversion systems such as solar cells and transparent conducting oxides.<sup>1,2</sup> The structure and morphology of ZnO are critical for the atomic-scale growth of nanomaterials.<sup>1,2</sup> Nanostructures have increased the range of potential application of ZnO; in particular, nanotubes, which are one-dimensional (1D) nanostructures, can be obtained using different methods of synthesis.

The first observation of the multiwall carbon nanotubes was credited to Iijima,<sup>3</sup> and in 1993, single-walled nanotubes were found by Iijima<sup>4</sup> and concurrently by Bethune.<sup>5</sup> Depending on how the sheet is wrapped, different nanotubes with singular properties can be obtained, thus opening new possibilities for further applications. These structures can be classified according to three main classes (based on chirality): armchair, zigzag, and chiral. The nanotube properties may change significantly depending on the chirality; for instance, armchair carbon nanotubes are always metallic, while the zigzag type can have a metallic or semiconducting character.<sup>6</sup>

Carbon nanotubes have been applied in different areas, but owing to the dependence of their electronic properties on their chirality, their application in semiconductors has not been very successful. For this reason, in recent years, other plausible

alternatives, such as inorganic nanotubes, have received increasing attention; in particular, inorganic nanotubes composed of metal oxides with morphology similar to that of carbon nanotubes have been explored. Among the several experimental techniques adopted to obtain inorganic nanotubes, a widely used method involves the material deposition onto an anodized aluminum oxide membrane template by using a collimated electron beam evaporation source.<sup>7</sup>

The synthesis of single-walled ZnO nanotubes (SWZnONTs) is influenced by the control of the synthesis route,<sup>8</sup> which leads to the improvement of the electrical and optical properties and is typically realized by using metal–organic chemical vapor deposition, also utilized by Xu et al.<sup>9</sup> to grow SWZnONTs on a Si substrate. Martinson et al.<sup>9</sup> used ZnO nanotubes as photoanodes in dye-sensitized solar cells, comparing them with other ZnO-based devices. The solar cells showed significant photovoltage and fill factor values and an efficiency up to 1.6%.

From a theoretical point of view, the three types of nanotubes can be easily obtained and simulated by adopting different techniques and theories. The simplicity to obtain a nanotube can be theoretically estimated by calculating the strain energy ( $E_s$ ), which considers the energy necessary to “wrap” a nanotube; thus, lower  $E_s$  values correspond to simple

Received: December 5, 2015

Revised: February 10, 2016

Published: March 4, 2016

nanotube fabrication. Notably,  $E_s$  can be calculated according to the equation [ $E_s = (E_{\text{nanotube}}/n_{\text{atoms}}) - E_{\text{slab}}$ ], where  $E_{\text{slab}}$  is the surface energy,  $E_{\text{nanotube}}$  is the energy of the nanotube, and  $n$  is the number of atoms of the nanotube. As a standard, some authors use the  $E_s$  values of the carbon nanotubes to compare  $E_s$  of other nanotubes, as carbon nanotubes are easily obtained.

Wang et al.<sup>10</sup> analyzed the stability and electronic structure of SWZnONTs using density functional theory (DFT) with the local density approximation (LDA) functional; they showed that the ZnO nanotube structure was very stable, experimentally attainable, and had smaller values of  $E_s$  than other nanotube structures reported in the literature, such as boron nitride and gallium nitride.

Concerning the stability, Shen et al.<sup>11</sup> studied SWZnONTs with a small diameter and compared them with nanobelts and nanowires. The analyzed nanotubes were more stable than other nanostructures but less stable than nanotubes with larger diameters.

Mirnezhad and co-workers<sup>12</sup> investigated the size and chirality dependence of the mechanical properties of ZnONTs for four different adsorption positions of the H atom. Poisson's ratio and Young's moduli were determined via DFT with LDA and showed that Young's modulus of the armchair nanotube was higher than those of the zigzag and chiral nanotubes.

Yan Su and co-workers<sup>13</sup> studied the adhesion of Pd nanoclusters on ZnONTs and the adsorption of probe gas molecules on the outside, or inside, wall of ZnO and Pd/ZnONTs using generalized gradient approximation (GGA). This study showed that the adsorption presents high energy inside the nanotube.

Molecular dynamics were performed to simulate the structural properties of zigzag, armchair, and chiral SWZnONTs.<sup>14</sup> After relaxation, all nanotube structures perfectly retained their ideal tube structures at 1 and 300 K, when periodic boundary conditions were used. On the other hand, when the strain was applied, the armchair and chiral nanotubes frequently assumed hexagonal and square geometries, while the zigzag nanotube assumed a hexagonal geometry.

Lacivita et al.<sup>15</sup> analyzed the bulk and (6,6) zigzag nanotube properties using DFT with PBE, B3LYP, LDA functional, and Hartree–Fock (HF) theory. They reported that for LDA and PBE the band gap of the nanotube was more than twice that of the bulk while for B3LYP, the value obtained for the nanotube was about 50% higher than that of the bulk HF overestimated by 15%. The vibrational modes of ( $n,n$ ) nanotubes were also calculated, but no direct correspondence was found in the vibrational spectrum of the monolayer surface.

Armchair and zigzag nanotubes were studied by Moraes et al.<sup>16</sup> with respect to length, diameter, and band gap using the AM1 semiempirical method; the results were then compared with those obtained with RHF/3-21G level. The band gap increased with the nanotube diameter and reached values of almost 9.0 eV for armchair and 1.0 eV for zigzag nanotubes. However, for zigzag nanotubes using AM1, a variation of the gap values appeared. Compared with other theoretical and experimental works, these results appeared overestimated.

Wang and co-workers<sup>10</sup> calculated the Zn–O bond length,  $E_s$ , and band gap for three types of SWZnONTs using GGA with exchange–correlation functional parametrized by PBE and showed that  $E_s$  decreased with the increase of the diameter nanotubes, while the band gap increased for all nanotubes to  $\sim 1.9$  eV, concluding that zigzag nanotubes were more stable than others.

These theoretical studies present different results and conclusions, indicating that this research area is still quite open and indefinite. Few theoretical studies have been devoted to ZnO nanotubes, and in general, these works report models for nanotubes of small diameter. Therefore, it is crucial to acquire knowledge and understanding by comparing the atomic-scale structural and electronic properties of this class of nanomaterials with the well-known properties of bulk and surfaces.

In this paper, periodic computational simulations are reported, based on DFT with the B3LYP, HSE06, PBE0, and PWGGA functional and all-electron basis set to investigate the structural, electronic, and vibrational properties of wurtzite ZnO single-walled armchair ( $n,n$ ) and zigzag ( $n,0$ ) nanotubes. A detailed study on the influence of the diameter of the nanotubes was carried out with respect to the bond length (Zn–O), bond angles (Zn–O–Zn), energy strain, band gap, density of states (DOS), band structures, and vibrational analysis. A topological analysis of the electron density,  $\rho(r)$ , was conducted according to the quantum theory of atoms in molecules (QTAIM) as developed by Bader<sup>17</sup> and implemented in the TOPOND code<sup>18</sup> for crystalline systems by Gatti.<sup>19,20</sup> The nanotubes properties were compared with the ZnO bulk and (0001) monolayer surface.

The nanotube models can be extended to study further issues, such as the effects caused by the addition of dopant and the interaction of molecules.

## ■ COMPUTING METHOD AND MODELS

All computational simulations of SWZnONTs were performed by periodic DFT using the CRYSTAL14 software.<sup>21</sup> CRYSTAL uses a Gaussian-type basis set to represent crystalline orbitals as a linear combination of Bloch functions defined in terms of local functions (atomic orbitals). The zinc and oxygen centers were described by 86-411d31G<sup>22</sup> and 8-411d1,<sup>23</sup> respectively.

The selected basis set is due to the fact that these have been used previously,<sup>24,25</sup> however, another available combination of basis set for Zn and, O atoms were tested and evaluated preliminarily. The choice of this basis set is considering the best approximation to the experimental band gap energy, lattice and internal parameters.

A very large grid with 99 radial points and 1454 angular points was adopted in the DFT integration. An overview of the algorithms used in the introduction of the DFT in the CRYSTAL computer code is presented by Towler and co-workers<sup>26</sup> and more details can be found in CRYSTAL user manual.<sup>21</sup> The level of accuracy in evaluating the infinite Coulomb and HF exchange series is controlled by five parameters,  $T_i = 1, 2, 3, 4$  and  $5$ , such that two-electron contributions are neglected when the overlap between atomic functions is below  $10^{-T_i}$ . For our calculations  $T_i$  have been set to 10, 10, 10, 20, and 40. The shrinking factor (Pack–Monkhorst and Gilat net) was set to 8, corresponding to 78 independent  $k$  points in the irreducible part of the Brillouin zone. For the surface calculations, the  $k$ -points mesh belongs to the  $xy$ -plane, whereas for nanotube calculations the  $k$ -points mesh acts on the periodic direction, i.e.,  $x$  direction. The choice of computational parameters can affect the results and quality of calculations. When more  $k$ -points are used, the sensitivity of the total energy becomes smoother. In particular, the results related to strain energy or surface energy can be sensitive to the convergence of total energy. This is an important step to the acknowledge the effect on the relevant quantities and properties.

In some cases, the surface energy can be modified and lead to erroneous conclusion about relative stability of surfaces when the K-grid does not present a smoother behavior. The same effect can be observed for total energy of nanotubes and strain energy. Therefore, the K-grid should be larger enough to have good cancellation of errors.

The band structures were obtained for 100 K points along the appropriate high-symmetry paths of the adequate Brillouin zone, and the DOS diagrams were calculated to analyze the corresponding electronic structure. The choice of the theoretical exploration of these systems is based on previous works by our research group.<sup>27,28</sup>

In general, computational simulations based on periodic DFT have a smaller computational cost than standard correlation methods. Therefore, an important step in the DFT calculation is the choice of the functional to be used in the simulation. Some functionals are able to predict the structure but underestimate the band gap; conversely, other functionals, which are able to accurately describe the band gap, tend often to overestimate the structural parameters. There are several comparative studies that examine the accuracy of the functionals in predicting the structural and electronic properties of molecules and solids.<sup>15,27</sup> The general conclusion is that none of the available functionals are able to simultaneously describe all electronic and structural properties of the studied systems. The successful for describing properties in solid state when these depended on accurate approximation on the band gap and band structure. In particular, the band gap energy is remarkable information that can bring the possible applications of materials. In this work, the B3LYP,<sup>29</sup> HSE06,<sup>30,31</sup> PBE0,<sup>32</sup> and PWGGA<sup>33</sup> functionals were used. B3LYP,<sup>29</sup> which is the most popular hybrid functional that mixes HF, LDA, and GGA, has shown good results when applied both to solid state and study of molecules.

The HSE06<sup>30,31</sup> functional is an hybrid short-range corrected functional where the correlation and exchange parts are evaluated at the PBE level with 0.25 of HF exchange and a screening parameter of  $\omega = 0.11 \text{ bohr}^{-1}$ .

The importance of including a certain percentage of exact HF exchange in order to better describe the effect of the quantum confinement in the description of band structure and dielectric properties has already been proved by Lacivita et al.<sup>15</sup> For this reason we have selected global and range-separated hybrid functionals to be compared with a pure gradient-corrected one.

As a first step, the optimizations of the lattice parameters and internal coordinates of wurtzite ZnO were conducted to minimize the total energy of the structure at experimental parameters. The ZnO wurtzite belongs to the space group  $P63mc$  with a Bravais lattice ( $a = 3.250 \text{ \AA}$  and  $c = 5.207 \text{ \AA}$ )<sup>34</sup> and can be depicted as planes of tetrahedrally coordinated oxygen and zinc atoms alternately stacked along the  $c$ -axis. The parameters calculated with the B3LYP functional were  $a = 3.274 \text{ \AA}$ ,  $c = 5.250 \text{ \AA}$ , and  $u = 0.383$ , which were in good agreement with the experimental values.

The structural parameters calculated with B3LYP were qualitatively analogous in the case of HSE06 and PBE0; on the other hand, the functional PWGGA overestimated the values of the structural parameters and internal parameter  $u$ .

From the bulk optimized parameters, the (0001) monolayer surface (periodic in the  $x$  and  $y$  directions) was built, and an optimization of the fractional coordinates was performed. Subsequently, the relaxed monolayer surface was wrapped in

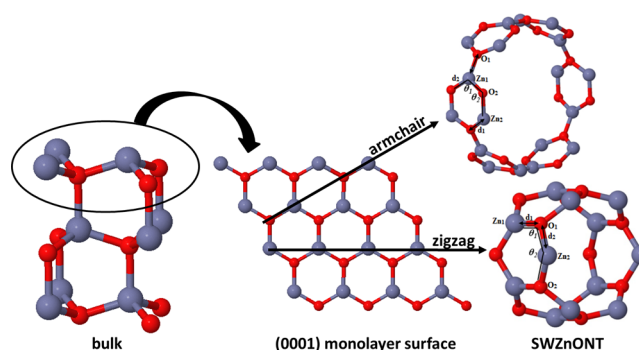


Figure 1. Schematic figure of the single-walled nanotube construction.

a 1D cylindrical structure (Figure 1), and the diameter and chirality of the system were defined by a vector  $(n,m)$  forming armchair  $(n,n)$  and zigzag  $(n,0)$  nanotubes with  $n = 4, 6, 8, 10, 12, 24, 48,$  and  $96$ , which correspond to diameters ranging from  $6$  to  $174 \text{ \AA}$ , which presents the same number of atoms.

The topological analysis of  $\rho(r)$  was obtained with the TOPOND program<sup>18</sup> incorporated in the CRYSTAL14 package. TOPOND has the advantages to exploit the full periodic theory of the former package so that it provides a new and reformulated version of chemical concepts at the same level of accuracy for systems periodic in any dimension, i.e., bulk, surfaces, and nanotubes.

The main instruments adopted in this work to analyze atomic interactions in the framework of Bader analysis are presented below; theoretical details can be found in works specifically devoted to topological analysis.<sup>35,36</sup> We will strictly focus on the determination and characterization of the so-called bond critical points whose properties allow for a unambiguous classification of chemical interactions.

A critical point (CP) in  $\rho(r)$  is a point where the gradient of the density vanishes,  $\nabla\rho(r) = 0$ . Each CP can be classified in terms of the eigenvalues,  $\lambda_1, \lambda_2,$  and  $\lambda_3$  of the Hessian matrix of the second-derivatives of  $\rho(r)$  evaluated at the CP; consequently, each CP can be labeled with two indices  $(r,s)$  where  $r$  is the number of nonzero  $\lambda_{(i=1,3)}$  values and  $s$  is the difference between positive and negative eigenvalues. Of peculiar interest are the bond critical points (BCP) corresponding to  $(3,-1)$  in terms of the  $(r,s)$  notation and indicating a saddle in the electron density scalar field, with a local minimum along the atom–atom direction and two maxima in the perpendicular directions.

Several quantities can be evaluated at BCP such as the Laplacian,  $\nabla^2\rho(r)$ , the potential energy density,  $V(r)$ , the positive definite kinetic energy density,  $G(r)$ , and the total electronic energy density,  $H(r) = V(r) + G(r)$ , in terms of which the bond degree,  $H(r)/\rho(r)$ , is defined. Moreover, the local formulation of the virial theorem establishes a fruitful relationship between some of them:

$$\frac{1}{4}\nabla^2\rho(r) = V(r) + 2G(r) = H(r) + G(r) \quad (1)$$

In terms of these descriptor, the nature of bond interactions can be rationalized as follows:<sup>20</sup> (i) covalent bonds exhibits negative Laplacian and  $H(r)$  and a  $V(r)/G(r)$  ratio larger than two as a consequence of an excess of potential energy at the BCP; (ii) transit bonds are associated with positive Laplacian, an almost zero value of the bond degree and  $1 < V(r)/G(r) < 2$ ; (iii) ionic, hydrogen bonds and van der Waals interactions

Table 1. Bond Length (Zn–O; Å) and Bond Angle (Zn–O–Zn; deg) of Armchair and Zigzag Nanotubes

		armchair				zigzag					
		B3LYP	HSE06	PBE0	PWGGA			B3LYP	HSE06	PBE0	PWGGA
(4,4)	$d_1$	1.89	1.88	1.88	1.94	(4,0)	$d_1$	1.86	1.84	1.84	1.91
	$d_2$	1.87	1.86	1.86	1.93		$d_2$	1.90	1.89	1.89	1.94
	$\alpha_1$	117.37	117.35	117.36	117.53		$\alpha_1$	105.18	105.14	105.13	105.44
	$\alpha_2$	120.29	120.34	120.34	119.97		$\alpha_2$	120.72	120.74	120.75	120.55
(6,6)	$d_1$	1.89	1.88	1.88	1.94	(6,0)	$d_1$	1.87	1.86	1.86	1.93
	$d_2$	1.88	1.87	1.87	1.94		$d_2$	1.89	1.88	1.88	1.94
	$\alpha_1$	118.83	118.81	118.81	118.89		$\alpha_1$	113.04	112.99	115.96	113.33
	$\alpha_2$	120.09	120.14	120.14	119.76		$\alpha_2$	120.30	120.32	120.18	120.13
(8,8)	$d_1$	1.89	1.88	1.88	1.94	(8,0)	$d_1$	1.88	1.87	1.87	1.94
	$d_2$	1.89	1.87	1.87	1.94		$d_2$	1.89	1.88	1.88	1.94
	$\alpha_1$	119.35	119.33	119.33	119.51		$\alpha_1$	113.04	115.97	117.39	116.33
	$\alpha_2$	120.02	120.08	120.08	119.69		$\alpha_2$	120.30	120.18	120.18	119.98
(10,10)	$d_1$	1.89	1.88	1.88	1.94	(10,0)	$d_1$	1.88	1.87	1.87	1.94
	$d_2$	1.89	1.87	1.87	1.95		$d_2$	1.89	1.88	1.88	1.94
	$\alpha_1$	119.59	119.57	119.57	119.76		$\alpha_1$	117.45	117.40	118.18	117.76
	$\alpha_2$	119.99	120.05	120.05	119.66		$\alpha_2$	120.09	120.11	120.07	119.92
(12,12)	$d_1$	1.89	1.88	1.88	1.94	(12,0)	$d_1$	1.89	1.87	1.87	1.94
	$d_2$	1.89	1.88	1.88	1.95		$d_2$	1.89	1.88	1.88	1.94
	$\alpha_1$	119.73	119.70	119.70	119.89		$\alpha_1$	118.23	118.19	118.18	118.55
	$\alpha_2$	119.98	120.03	120.03	119.64		$\alpha_2$	120.05	120.07	120.07	119.88
(24,24)	$d_1$	1.89	1.88	1.88	1.94	(24,0)	$d_1$	1.89	1.88	1.88	1.95
	$d_2$	1.89	1.88	1.88	1.95		$d_2$	1.89	1.88	1.88	1.93
	$\alpha_1$	119.95	119.93	119.93	120.12		$\alpha_1$	119.60	119.55	119.55	119.93
	$\alpha_2$	119.95	120.00	120.00	119.61		$\alpha_2$	119.99	120.02	120.02	119.82
(48,48)	$d_1$	1.89	1.88	1.88	1.94	(48,0)	$d_1$	1.89	1.88	1.88	1.95
	$d_2$	1.89	1.88	1.88	1.95		$d_2$	1.89	1.88	1.88	1.93
	$\alpha_1$	120.01	119.99	119.99	120.18		$\alpha_1$	119.95	119.90	119.89	120.28
	$\alpha_2$	119.94	119.99	119.99	119.61		$\alpha_2$	119.97	120.00	120.00	119.81
(96,96)	$d_1$	1.89	1.88	1.88	1.94	(96,0)	$d_1$	1.89	1.88	1.88	1.95
	$d_2$	1.89	1.88	1.88	1.95		$d_2$	1.89	1.88	1.88	1.93
	$\alpha_1$	120.03	120.00	120.00	120.19		$\alpha_1$	120.03	119.98	119.98	120.37
	$\alpha_2$	119.94	119.99	119.99	119.60		$\alpha_2$	119.97	120.00	120.00	119.80

show positive Laplacian and  $H(r)$  and a  $V(r)/G(r)$  ratio lower than 1 due to the dominance of kinetic energy at the BPC.

Integration of the charge density over the atomic basins gives further information such as atomic volume, Bader's atomic charges, and the partition of the energy in atomic contributions.

In this work, CPs have been searched using the eigenvector-following approach<sup>36</sup> and the Morse relationship

$$\mathbf{n}_{3,-3} - \mathbf{n}_{3,-1} + \mathbf{n}_{3,+1} - \mathbf{n}_{3,+3} = 0 \quad (2)$$

where  $\mathbf{n}$  identify the number of CP has been verified *a posteriori* and is fulfilled for all the structures.

## RESULTS AND DISCUSSION

**Structural Properties.** The calculated Zn–O bond length and angle in armchair and zigzag SWZnONTs (Figure 1) are reported in Table 1. The calculated bond length was approximately 1.89 Å for B3LYP, HSE06, and PBE0 and 1.94 Å for PWGGA. The average Zn–O–Zn bond angle for all nanotubes was 119° for all functionals. These parameters are similar to those of the (0001) monolayer surface but different from the bond length and angle observed in ZnO bulk, which are equal to 1.99 Å and 108.26°, respectively. When the nanotube diameter increases, the structure approaches the monolayer surface.

These results were also observed by other authors. Lacivita et al.<sup>15</sup> analyzed the armchair nanotubes from (4,4) to (50,50) and showed that the bond length of the (50,50) nanotube was

1.8970 Å, while that of the monolayer was 1.8969 Å, in good agreement with the results obtained in this work. Zhou and co-workers<sup>37</sup> reported zigzag nanotubes with a structure very similar to that obtained for the (0001) surface and comparable to that of carbon nanotubes. Krainara et al.<sup>38</sup> analyzed the structure of ZnS zigzag single-walled nanotubes; the structure obtained after the optimization closely resembled that obtained for the surface, excluding the lower smoothness. These works are in good agreement with this study in relation to the results obtained for nanotubes as well as bulk and surface.

The  $E_s$  values of the nanotubes were calculated with all functionals and are reported in Table 2. For both nanotube types, a decrease of  $E_s$  with the increase of the nanotube diameter could be observed (see Figure 2), showing a stabilization in (12,12) and (12,0) nanotubes. Nanotubes with a large diameter are formed easier than those with a small diameter. All functionals showed the same behavior.

The  $E_s$  values for zigzag nanotubes are slightly higher than the values calculated for armchair nanotubes; the small difference, only 0.01 eV/atom, may depend on the methodology or the error accumulation in the numerical calculation process; both can be obtained experimentally, depending of the experimental conditions. Xu and coauthors<sup>39</sup> synthesized two types of ZnO nanotubes on a Si substrate; the present study suggests that they were armchair and zigzag type nanotubes. However, Wang et al.<sup>10</sup> performed a theoretical study on ZnO

Table 2. Energy Strain ( $E_s$ ; eV/Atom) and Band Gap Energy ( $E_{\text{gap}}$ ; eV) for Nanotubes, Bulk, and (0001) Monolayer Surface

nanotube	B3LYP		HSE06		PBE0		PWGGA	
	$E_s$	$E_{\text{gap}}$	$E_s$	$E_{\text{gap}}$	$E_s$	$E_{\text{gap}}$	$E_s$	$E_{\text{gap}}$
(4,4)	0.050	4.42	0.050	4.30	0.050	5.04	0.044	2.14
(6,6)	0.021	4.50	0.021	4.37	0.021	5.10	0.018	2.19
(8,8)	0.013	4.51	0.013	4.39	0.013	5.13	0.010	2.21
(10,10)	0.009	4.52	0.009	4.40	0.009	5.14	0.007	2.22
(12,12)	0.006	4.53	0.006	4.41	0.007	5.15	0.005	2.23
(24,24)	0.002	4.54	0.002	4.42	0.002	5.16	0.000	2.23
(48,48)	0.001	4.54	0.001	4.42	0.001	5.16	-0.001	2.24
(96,96)	0.001	4.54	0.000	4.42	0.001	5.16	-0.001	2.24
(4,0)	0.199	4.23	0.197	4.10	0.198	4.86	0.178	2.01
(6,0)	0.074	4.39	0.073	4.26	0.074	5.01	0.065	2.13
(8,0)	0.038	4.45	0.038	4.33	0.038	5.08	0.033	2.19
(10,0)	0.024	4.49	0.023	4.36	0.024	5.11	0.020	2.21
(12,0)	0.017	4.50	0.017	4.38	0.017	5.12	0.014	2.21
(24,0)	0.005	4.54	0.005	4.41	0.005	5.15	0.003	2.23
(48,0)	0.002	4.54	0.002	4.42	0.002	5.16	0.000	2.24
(96,0)	0.001	4.54	0.001	4.42	0.001	5.16	-0.001	2.24
bulk		3.21		2.99		3.69		1.06
surface		4.56		4.42		5.17		2.23

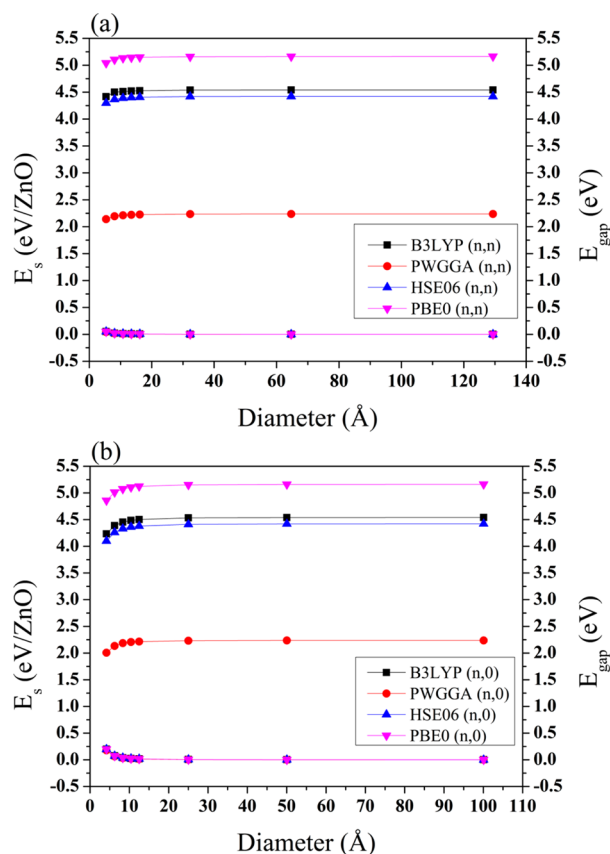


Figure 2. Energy strain and Band gap energy as functions of the nanotube diameter: (a) armchair; (b) zigzag.

nanotubes, indicating that ZnO zigzag nanotubes were the most stable, but only a slight difference between the  $E_s$  values of armchair and zigzag nanotubes could be observed for nanotubes with the same diameter.

**Electronic Properties.** Figure S1 shows the band structure and the total and projected DOS of ZnO bulk for all functionals. The shape of the band structure and DOS are qualitatively similar at all levels of theory. Upon analysis of the

calculated structural parameter, band gap energy, surface energy, elastic constants, and piezoelectric constants, the functional B3LYP showed the best results; thus, we chose to present the results for this functional. For this reason, the discussion refers to the B3LYP functional.

In bulk ZnO, the top of the valence band (VB), coincident with the Fermi level energy ( $-5.47$  eV), is located at the  $\Gamma$  point. The band gap is direct, 3.21 eV, in accordance with the experimental optically measured gap and other theoretical works. An analysis of the DOS of the bulk model, shown in Figure S1b, indicates that the VB consists mainly of 2p levels of O atoms, and the intense peak is due to 3d orbitals of Zn atoms. The main contribution of the conduction band (CB) comes from 4s4p levels of Zn atoms. The calculated band gap for the PWGGA level is considerably lower than that predicted experimentally and the values calculated with the B3LYP, HSE06, and PBE0 functionals. This underestimation is expected, as the exchange-correlation functionals within the GGA family are known to fail in describing the semiconductor character of some solids. However, the LDA and PBE functionals were previously tested for bulk. The calculated band gap energy, 0.89 and 1.05 eV, with LDA and PBE, respectively, were underestimated.

The optimized (0001) monolayer surface also exhibited a direct band gap, 4.56 eV for B3LYP, at  $\Gamma$  point (Figure S2), and a similar contribution of the atomic orbital, with major contributions from oxygen at the VB and zinc at the CB.

The results presented in Table 2 show the values of  $E_{\text{gap}}$  of the nanotubes.  $E_{\text{gap}}$  increased from 4.42 to 4.54 eV for (4,4) and (96,96), respectively, and from 4.23 to 4.53 eV for (4,0) and (96,0), respectively. The HSE06 functional showed similar values of  $E_{\text{gap}}$ , whereas PBE0 produced overestimated values (see Table 2); PWGGA presented values well below those obtained with the other functionals.

Figures 3 and 4 shows the band structure and DOS at B3LYP level for three selected models of armchair ((6,6), (12,12), and (24,24)) and zigzag ((6,0), (12,0), and (24,0)) nanotubes, respectively. All nanotubes have a direct band gap at the  $\Gamma$  point, coincident with the observed direct bad gap for bulk and (0001) monolayer surface.

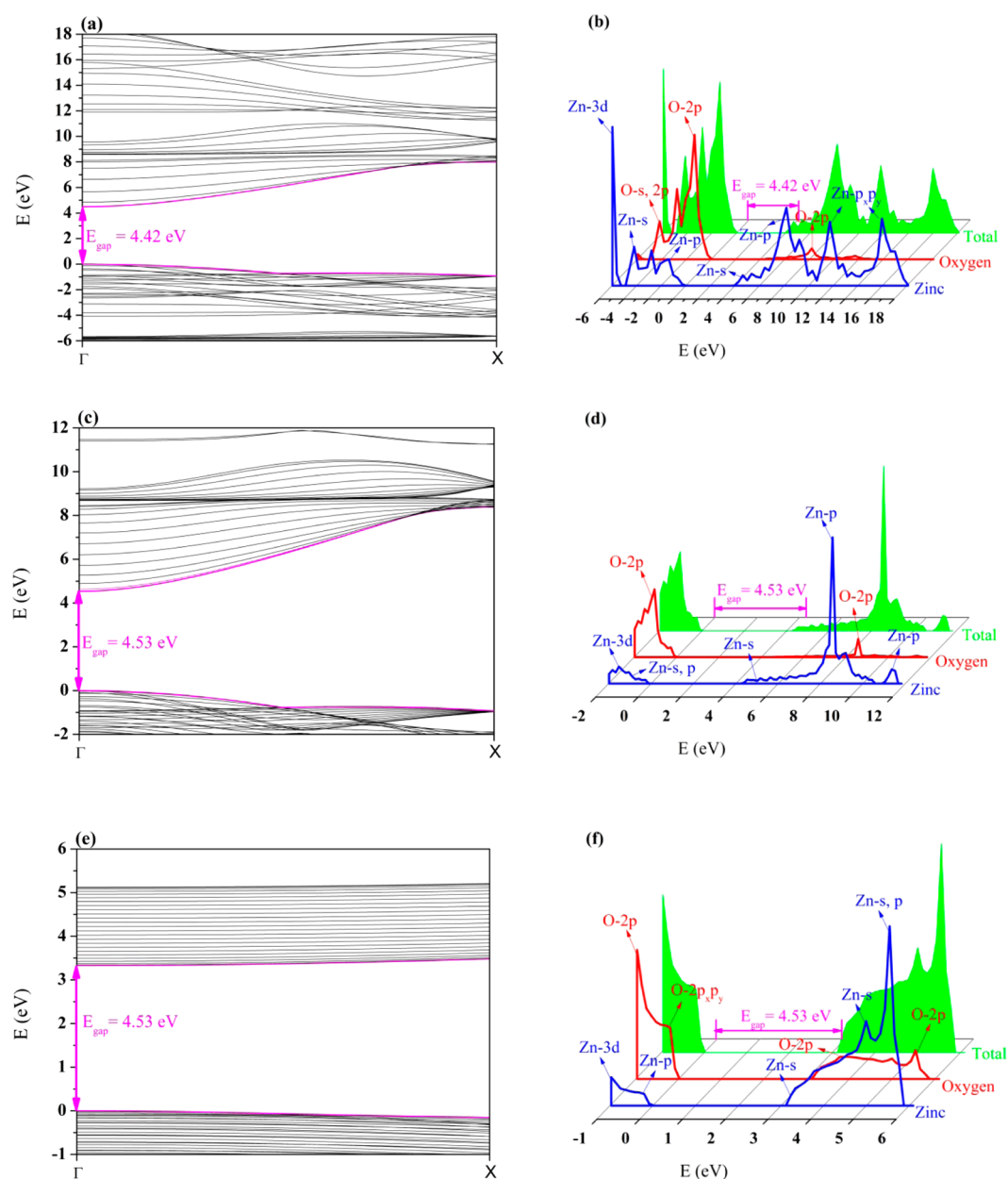


**Figure 3.** Band structure and density of states of armchair nanotubes: (a, b) (6,6); (c, d) (12,12); (e, f) (24,24).

The band structures for models with larger diameters are very similar and remain concentrated near the top and bottom of the VB and CB, respectively. The DOS analysis showed a major contribution of the  $2p_y$  and  $2p_z$  orbitals of oxygen atoms in the top of the VB band and  $3d$  orbitals of zinc atom in the intermediate region of the VB. In the CB, the contributions of  $s$  and  $p$  orbitals of zinc atoms were observed.

In general, the calculated band gaps of the nanotubes are greater than  $E_{\text{gap}}$  of the bulk and have a similar value to that of the (0001) monolayer surface. The band gap value converges to 4.54 eV.

The calculated Bader atomic charges for all nanotubes were 1.29 and  $-1.29$  au for the zinc and oxygen atoms, respectively. For comparison, the Mulliken charges analysis was conducted. The calculated values for all models of armchair and zigzag nanotubes were 0.883 and  $-0.883$  au for zinc and oxygen atoms, respectively. Both nanotubes present Bader and Mulliken atomic charges very close to the (0001) monolayer surface.

Notably, the values obtained for both population analyses cannot be directly compared with respect to their magnitude but can be compared for tendency. Indeed, there is not a unique method to obtain the atomic charge on each atom, which is dependent on the basis set and the method of calculation. In particular, the Mulliken charges, which are not based on density analyses, can be directly obtained from the corresponding wave function of that atom. However, this is not quite accurate because of the overlapping of the wave functions of neighboring atoms.

**Vibrational Properties.** The vibrational spectra of infrared (IR) and Raman, and the corresponding modes, for bulk, (0001) monolayer surface, (12,12), and (12,0) nanotubes, are shown in Figures S3–S6; no shifts are made.

ZnO bulk presents two IR-active modes, located at  $389.34\text{ cm}^{-1}$  (A, oxygen wagging) and  $417.65\text{ cm}^{-1}$  (E, oxygen scissoring), and four Raman-active modes,  $104.92\text{ cm}^{-1}$  (E, Zn–O twisting),  $389.34\text{ cm}^{-1}$  (A, oxygen wagging),

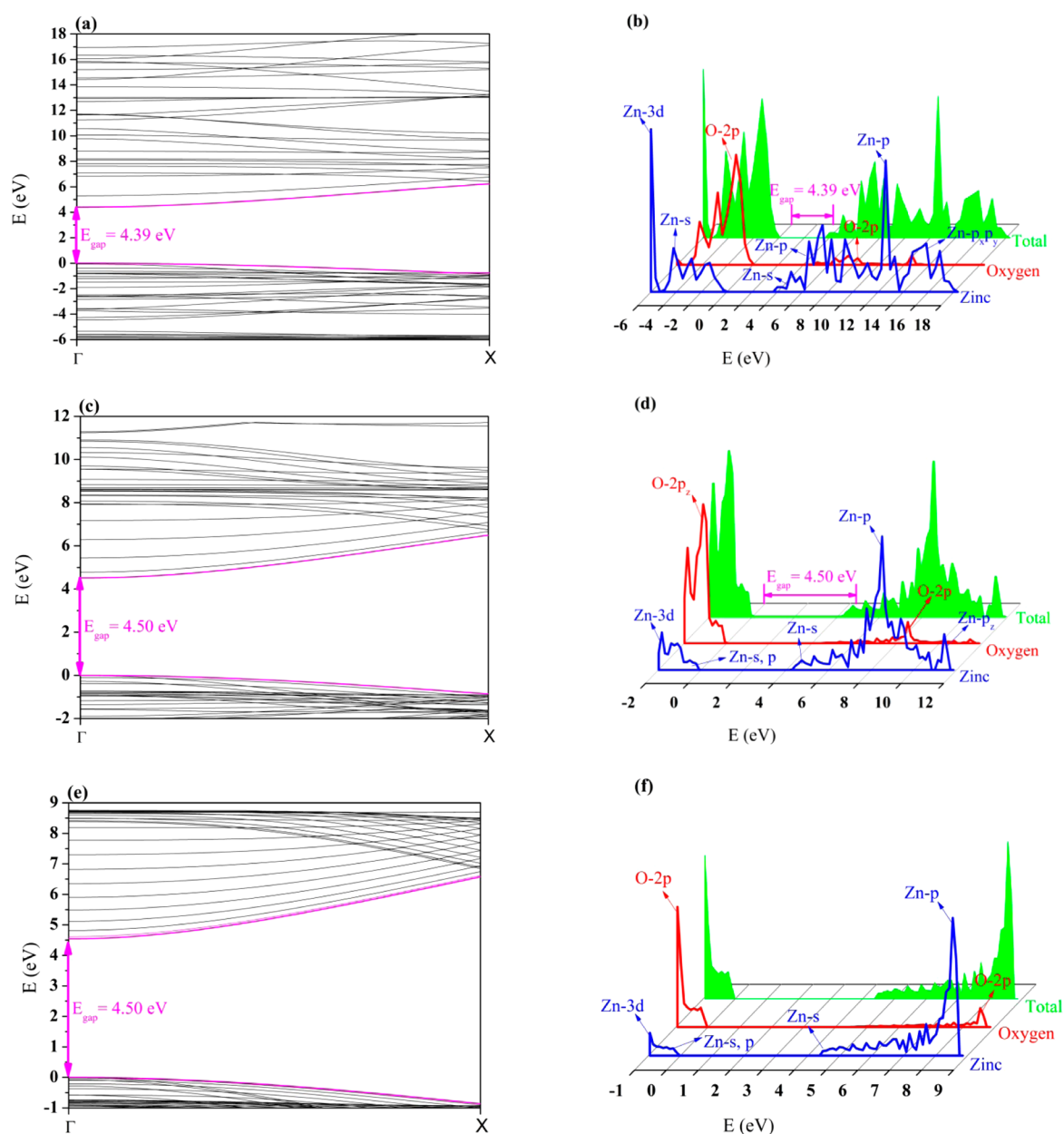


**Figure 4.** Band structure and density of states of zigzag nanotubes: (a, b) (6,0); (c, d) (12,0); (e, f) (24,0).

417.65  $\text{cm}^{-1}$  ( $E$ , oxygen scissoring), and 441.90  $\text{cm}^{-1}$  ( $E$ , oxygen twisting). For the (0001) monolayer surface, there are similar assignment movements, both active in IR and Raman, located at 302.47  $\text{cm}^{-1}$  ( $A$ , oxygen wagging) and 555.41  $\text{cm}^{-1}$  ( $E$ , oxygen scissoring).

For the (12,12) nanotube, there are three IR-active modes, 290.56  $\text{cm}^{-1}$  ( $E'_3$ , oxygen wagging), 558.86  $\text{cm}^{-1}$  ( $A'_w$  oxygen rocking), and 620.65  $\text{cm}^{-1}$  ( $E'_3$ , oxygen scissoring), and six Raman-active modes, 90.71  $\text{cm}^{-1}$  ( $E'_5$ , Zn–O stretching), 278.72  $\text{cm}^{-1}$  ( $E'_5$ , oxygen wagging), 301.27  $\text{cm}^{-1}$  ( $A'_g$  oxygen wagging), 559.96  $\text{cm}^{-1}$  ( $E'_3$ , Zn–O stretching), 562.31  $\text{cm}^{-1}$  ( $A'_g$ , oxygen rocking), and 650.54  $\text{cm}^{-1}$  ( $E'_5$ , oxygen scissoring). No corresponding modes of IR and Raman were observed.

The (12,0) nanotube present  $2A_1 + 2E_5$  IR and Raman-active modes, 282.63  $\text{cm}^{-1}$  ( $E_5$ , oxygen wagging), 527.24  $\text{cm}^{-1}$  ( $A_1$ , oxygen rocking), 576.27  $\text{cm}^{-1}$  ( $A_1$ , oxygen wagging) and 640.17  $\text{cm}^{-1}$  ( $E_5$ , oxygen scissoring), and  $E_5 + E_{10}$  only Raman

active, 28.46  $\text{cm}^{-1}$  ( $E_5$ , O rocking), 144.90  $\text{cm}^{-1}$  ( $E_{10}$ , Zn–O stretching).

There are no similar assignment movements for armchair and zigzag nanotubes. The modes of both SWZnONT do not have any direct correspondence in the vibrational spectrum of the (0001) monolayer surface and bulk.

The Raman and IR data can be used to provide a fingerprint by which the chirality of nanotubes can be indentified in experimental research.

**Topological Analysis.** The topological analysis of the electron density (Table 3), in particular as regards the properties of  $\rho(r)$  at the BCP, can provide important information on chemical bonds, fundamental to understand the type of interaction between two atoms and the modification induced by structure rearrangements.

The main effects on charge topology and Zn–O interaction emerge as the surface is formed and are strictly related to the decrease in the coordination sphere of both the atoms.

**Table 3. Several Properties (Electron Charge Density, Its Laplacian, the  $V/G$  Ratio, and the Bond Degree  $H/\rho(r)$ , and Ellipticity, All in Atomic Units) Computed at the Zn–O Bond Critical Point in Different Structures at the B3LYP Level<sup>a</sup>**

	topological properties								charges				volume
	$d_1$	$d_{\text{BCP}}$		$\rho(r)$	$\nabla^2\rho$	$V/G$	$H/\rho(r)$	$\varepsilon$	Mulliken		Bader		Bader
		Zn	O						Zn	O	Zn	O	O (%)
bulk	1.99	0.96	1.04	0.08	0.41	1.06	−0.08	0	0.914	−0.914	1.30	−1.30	57
surface	1.89	0.92	0.97	0.10	0.59	1.06	−0.09	0.029	0.884	−0.884	1.27	−1.27	55
(24,24)	1.89	0.92	0.97	0.10	0.59	1.06	−0.09	0.029	0.885	−0.885	1.27	−1.27	55
(24,0)	1.89	0.92	0.97	0.10	0.59	1.06	−0.10	0.029	0.885	−0.885	1.27	−1.27	55
(4,4)	1.87	0.91	0.95	0.10	0.63	1.06	−0.10	0.027	0.883	−0.883	1.27	−1.27	55
	1.89	0.92	0.97	0.10	0.58	1.06	−0.09	0.029	0.883	−0.883	1.27	−1.27	55
(4,0)	1.86	0.91	0.95	0.11	0.66	1.07	−0.11	0.018	0.883	−0.883	1.27	−1.27	54
	1.90	0.92	0.98	0.10	0.57	1.06	−0.10	0.032	0.883	−0.883	1.27	−1.27	54

<sup>a</sup>Bond distances as well as Mulliken and Bader charges are reported for sake of comparison; distances are in angstroms. The percentage of oxygen volume, as evaluated by the integration of the charge over the atomic basin, with respect to the total Zn plus O is also given.

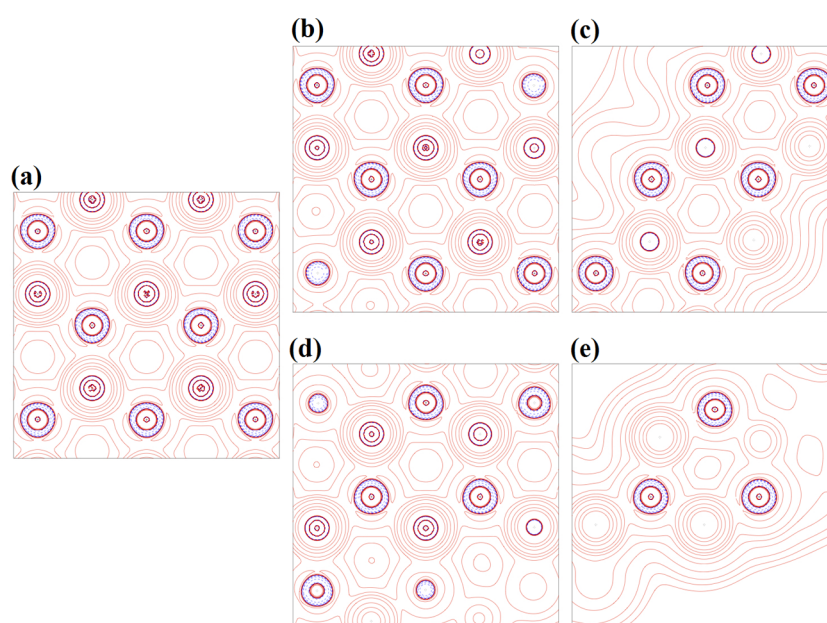


**Figure 5.** Laplacian of the electron density in the plane containing the oxygen atoms evaluated at the B3LYP level. (a) ZnO monolayer, (b) armchair (24,24), (c) (4,4) and (d) zigzag (24,0), (e) (4,0). A logarithmic scale is adopted between  $-8.0$  and  $8.0$  au. Continuous red and dotted blue lines indicate positive and negative contour levels, respectively.

Although the significant structural deformation, it seems that bond framework and charge density are not very much perturbed. As surface occurs, the Zn–O distance is shortened, the charge is slightly less polarized between the two atoms, and the volume of the anion is sensitively reduced with respect to that of Zn. By the point of view of main topological properties (24,24) and (24,0) tubes are almost indistinguishable from the monolayer, and this can also be seen looking at Figure 5 where the values of the Laplacian,  $\nabla^2\rho$ , in the plane containing the oxygen atoms are plotted and compared with the surface ones. In these case, regions of charge depletion and concentration are equally presented and electronic distribution seems not affected by the finite dimension of the (24,24) and (24,0) surface. The few deformations appearing in (4,4) and (4,0) Laplacian only involve the valence region of the shell structure of the atoms closest to the border but do not change significantly the Zn–O bond nature.

Indeed, topological indicators support for all the systems the general description of the ZnO bond as belonging to the

transit region, so neither ionic nor covalent. BCPs are almost equidistant from the two nuclear attractors, and negative bond degrees, although small in absolute values, indicate a local excess of potential energy, as for covalent bonds; also the very small values of ellipticity,  $\varepsilon$ , highlight the cylindrically symmetric shape of the bonds and their poor directionality. On the other hand, BCP densities around  $0.1 \text{ e/bohr}^3$  and positive values of the Laplacian suggest a ionic nature of the Zn–O bond.

Interesting enough, in the smaller nanotubes, (4,4) and (4,0), the two Zn–O bonds that according to Table 1 have different length exhibit sensitive differences in the topology, in particular as regards Laplacian and ellipticity.

Finally, Bader approach represents structures where the lowering in the dimensionality (passing from bulk to surfaces) is accomplished with a decreasing of the atomic charge whereas Mulliken analysis lands at an opposite description, as already stated in the Electronic Properties section.

## CONCLUSION

Periodic DFT calculations with B3LYP, HSE06, PDE0, and PWGGA functionals and all-electron Gaussian basis set were performed to simulate the structural and electronic properties of armchair and zigzag SWZnONTs with different diameters.

The results obtained with B3LYP and HSE06 presents similar values of bond length, bond angle,  $E_s$ , and  $E_{\text{gap}}$ ; however, PWGGA functional overestimated all mentioned parameters cited above.

The calculated  $E_s$  values of nanotubes with all functionals showed a decrease behavior with the increase of the nanotube diameter; however, the  $E_s$  stabilizes in (12,12) and (12,0) nanotubes, concluding that large diameter nanotubes are formed easier than those with a small diameter.

The calculated  $E_{\text{gap}}$  of the SWZnONT are greater than  $E_{\text{gap}}$  of the bulk and have a similar value to (0001) monolayer surface. The  $E_{\text{gap}}$  values of nanotubes converge to 4.54 eV, maintaining the semiconductor character.

The band structures for models with larger diameters are very similar and remain concentrated near the top and bottom of the VB and CB, respectively. The DOS analysis showed a major contribution of the  $2p_y$  and  $2p_z$  orbitals of oxygen atoms in the top of the VB band, and  $3d$  orbitals of zinc atom in the intermediate region of the VB. In the CB, the contributions of  $s$  and  $p$  orbitals of zinc atoms were observed.

The bulk and (0001) monolayer surface presents two similar assignment movements, both active in IR and Raman. However, there are no similar assignment movements for armchair and zigzag nanotubes, and the modes of both SWZnONT do not have any direct correspondence in the vibrational spectrum of the (0001) monolayer surface and bulk.

Zn–O bond length and bond angle, Mulliken and Bader charges, and all topological descriptors of ZnO interaction nanotubes of both chirality are similar to the same quantities as computed for the (0001) monolayer surface.

Owing to these analyses, both chiralities with large diameter can be used interchangeably in semiconductor applications. These theoretical models can be extended and applied to other computational simulations, as doping or adsorption process.

## ASSOCIATED CONTENT

### Supporting Information

The Supporting Information is available free of charge on the ACS Publications website at DOI: 10.1021/acs.jpcc.5b11905.

Band structure and density of states of ZnO bulk and monolayer surface (0001); vibrational IR and Raman spectra (PDF)

## AUTHOR INFORMATION

### Corresponding Author

\*E-mail: sambrano@fc.unesp.br (J.R.S.).

### Notes

The authors declare no competing financial interest.

## ACKNOWLEDGMENTS

This work is supported by Brazilian Funding Agencies: CNPq, CAPES, FAPESP (2013/19289-0, 2013/19713-7, 2013/07296-2). The computational facilities were supported by resources supplied by Molecular Simulations Laboratory, São Paulo State University, Bauru, Brazil.

## REFERENCES

- (1) Ozgur, U.; Alivov, Y. I.; Liu, C.; Teke, A.; Reshchikov, M. A.; Dogan, S.; Avrutin, V.; Cho, S. J.; Morkoc, H. A Comprehensive Review of ZnO Materials and Devices. *J. Appl. Phys.* **2005**, *98*, 041301.
- (2) Ozgur, U.; Hofstetter, D.; Morkoc, H. ZnO Devices and Applications: A Review of Current Status and Future Prospects. *Proc. IEEE* **2010**, *98*, 1255–1268.
- (3) Iijima, S. Helical Microtubules of Graphitic Carbon. *Nature* **1991**, *354*, 56–58.
- (4) Iijima, S.; Ichihashi, T. Single-shell Carbon Nanotubes of 1-nm Diameter. *Nature* **1993**, *364*, 737–737.
- (5) Bethune, D. S.; Klang, C. H.; Devries, M. S.; Gorman, G.; Savoy, R.; Vazquez, J.; Beyers, R. Cobalt-catalyzed Growth of Carbon Nanotubes with Single-atomic-layerwalls. *Nature* **1993**, *363*, 605–607.
- (6) Thostenson, E. T.; Ren, Z. F.; Chou, T. W. Advances in the Science and Technology of Carbon Nanotubes and their Composites: A Review. *Compos. Sci. Technol.* **2001**, *61*, 1899–1912.
- (7) Dickey, M. D.; Weiss, E. A.; Smythe, E. J.; Chiechi, R. C.; Capasso, F.; Whitesides, G. M. Fabrication of Arrays of Metal and Metal Oxide Nanotubes by Shadow Evaporation. *ACS Nano* **2008**, *2*, 800–808.
- (8) Kim, S. B.; Kim, S.; Kwon, S. S.; Lee, W. W.; Kim, J.-S.; Park, W. I. Large-Scale Synthesis of Vertically Aligned ZnO Hexagonal Nanotube-Rod Hybrids Using a Two-Step Growth Method. *J. Am. Ceram. Soc.* **2013**, *96*, 3500–3503.
- (9) Martinson, A. B. F.; Elam, J. W.; Hupp, J. T.; Pellin, M. J. ZnO nanotube based dye-sensitized solar cells. *Nano Lett.* **2007**, *7*, 2183–2187.
- (10) Wang, B.; Nagase, S.; Zhao, J.; Wang, G. The Stability and Electronic Structure of Single-walled ZnO Nanotubes by Density Functional Theory. *Nanotechnology* **2007**, *18*, 345706.
- (11) Shen, X.; Allen, P. B.; Muckerman, J. T.; Davenport, J. W.; Zheng, J.-C. Wire versus Tube: Stability of Small One-dimensional ZnO Nanostructures. *Nano Lett.* **2007**, *7*, 2267–2271.
- (12) Mirnezhad, M.; Ansari, R.; Rouhi, H. Effects of hydrogen adsorption on mechanical properties of chiral single-walled zinc oxide nanotubes. *J. Appl. Phys.* **2012**, *111*, 014308.
- (13) Su, Y.; Meng, Q.-q.; Wang, J.-g. A DFT Study of the Adhesion of Pd Clusters on ZnO SWNTs and Adsorption of Gas Molecules on Pd/ZnO SWNTs. *J. Phys. Chem. C* **2009**, *113*, 21338–21341.
- (14) Kilic, M. E.; Erkoç, S. Structural Properties of ZnO Nanotubes Under Uniaxial Strain: Molecular Dynamics Simulations. *J. Nanosci. Nanotechnol.* **2013**, *13*, 6597–6610.
- (15) Lacivita, V.; Erba, A.; Noel, Y.; Orlando, R.; D'Arco, P.; Dovesi, R. Zinc oxide nanotubes: An Ab Initio Investigation of their Structural, Vibrational, Elastic, and Dielectric Properties. *J. Chem. Phys.* **2013**, *138*, 214706.
- (16) de Moraes, E.; Gargano, R.; Politi, J. R.; de Castro, E. A. S.; dos Santos, J. D.; Longo, E.; Taft, C. A.; Martins, J. B. L. A Theoretical Investigation of ZnO Nanotubes: Size and Diameter. *Curr. Phys. Chem.* **2013**, *3*, 400–407.
- (17) Bader, R. F. W. *Atoms in Molecules - A Quantum Theory*; Oxford University Press: Oxford, 1990.
- (18) Gatti, C.; Casassa, S. *TOPOND User's Manual*, CNR-CSR SRC, Milano, 2013.
- (19) Gatti, C.; Saunders, V. R.; Roetti, C. Crystal-field Effects on the Topological Properties of the Electron-density in Molecular-crystals - The Case of Urea. *J. Chem. Phys.* **1994**, *101*, 10686–10696.
- (20) Gatti, C. Chemical Bonding in Crystals: New Directions. *Z. Kristallogr. - Cryst. Mater.* **2005**, *220*, 399–457.
- (21) Dovesi, R.; Saunders, V. R.; Roetti, C.; Orlando, R.; Zicovich-Wilson, C. M.; Pascale, F.; Civalieri, B.; Doll, K.; Harrison, N. M.; Bush, I. J.; D'Arco, P.; Llunell, M.; Causà, M.; Noël, Y. *CRYSTAL14 User's Manual*; University of Torino: Torino, 2014.
- (22) Jaffe, J. E.; Hess, A. C. Hartree-Fock study of Phase-changes in ZnO at High-pressure. *Phys. Rev. B: Condens. Matter Mater. Phys.* **1993**, *48*, 7903–7909.
- (23) Bredow, T.; Jug, K.; Evarestov, R. A. Electronic and Magnetic Structure of ScMnO<sub>3</sub>. *Phys. Status Solidi B* **2006**, *243*, R10–R12.

(24) Lima, R. C.; Macario, L. R.; Espinosa, J. W. M.; Longo, V. M.; Erlo, R.; Marana, N. L.; Sambrano, J. R.; dos Santos, M. L.; Moura, A. P.; Pizani, P. S.; Andres, J.; Longo, E.; Varela, J. A. Toward an Understanding of Intermediate and Short-range Defects in ZnO Single Crystals. A Combined Experimental and Theoretical Study. *J. Phys. Chem. A* **2008**, *112*, 8970–8978.

(25) Marana, N. L.; Longo, V. M.; Longo, E.; Martins, J. B. L.; Sambrano, J. R. Electronic and Structural Properties of the (10 $\bar{1}$ )over-bar0 and (11 $\bar{2}$ )over-bar0 ZnO Surfaces. *J. Phys. Chem. A* **2008**, *112*, 8958–8963.

(26) Towler, M. D.; Zupan, A.; Causa, M. Density Functional Theory in Periodic Systems Using Local Gaussian Basis Sets. *Comput. Phys. Commun.* **1996**, *98*, 181–205.

(27) Albuquerque, A. R.; Maul, J.; Longo, E.; dos Santos, I. M. G.; Sambrano, J. R. Hydrostatic and 001 Uniaxial Pressure on Anatase TiO<sub>2</sub> by Periodic B3LYP-D\* Calculations. *J. Phys. Chem. C* **2013**, *117*, 7050–7061.

(28) Moura, K. F.; Maul, J.; Albuquerque, A. R.; Casali, G. P.; Longo, E.; Keyson, D.; Souza, A. G.; Sambrano, J. R.; Santos, I. M. G. TiO<sub>2</sub> Synthesized by Microwave Assisted Solvothermal Method: Experimental and Theoretical Evaluation. *J. Solid State Chem.* **2014**, *210*, 171–177.

(29) Becke, A. D. Density-functional Thermochemistry 0.3. The Role of Exact Exchange. *J. Chem. Phys.* **1993**, *98*, 5648–5652.

(30) Heyd, J.; Scuseria, G. E.; Ernzerhof, M. Hybrid Functionals Based on a Screened Coulomb Potential. *J. Chem. Phys.* **2003**, *118*, 8207–8215.

(31) Heyd, J.; Scuseria, G. E.; Ernzerhof, M. Hybrid Functionals Based on a Screened Coulomb Potential. *J. Chem. Phys.* **2006**, *124*, 219906.

(32) Adamo, C.; Barone, V. Toward Reliable Density Functional Methods Without Adjustable Parameters: The PBE0Model. *J. Chem. Phys.* **1999**, *110*, 6158–6170.

(33) Perdew, J. P.; Chevary, J. A.; Vosko, S. H.; Jackson, K. A.; Pederson, M. R.; Singh, D. J.; Fiolhais, C. Atoms, Molecules, Solids and Surfaces: Applications of the Generalized Approximation for Exchange and Correlation. *Phys. Rev. B: Condens. Matter Mater. Phys.* **1992**, *46*, 6671.

(34) Decremps, F.; Datchi, F.; Saitta, A. M.; Polian, A.; Pascarelli, S.; Di Cicco, A.; Itie, J. P.; Baudelet, F. Local Structure of Condensed Zinc Oxide. *Phys. Rev. B: Condens. Matter Mater. Phys.* **2003**, *68*, 104101.

(35) Bader, R. F. W. The Role of Atoms in Molecules. *Abstr. Pap. Am. Chem. Soc.* **1994**, *207*, 246–ORGN.

(36) Popelier, P. L. A. A Robust Algorithm to Locate Automatically all Types of Critical-points in the Charge-density and its Laplacian. *Chem. Phys. Lett.* **1994**, *228*, 160–164.

(37) Zhou, Z.; Li, Y.; Liu, L.; Chen, Y.; Zhang, S. B.; Chen, Z. Size and Surface-dependent Stability, Electronic Properties, and Potential as Chemical Sensors: Computational Studies on One-dimensional ZnO Nanostructures. *J. Phys. Chem. C* **2008**, *112*, 13926–13931.

(38) Krainara, N.; Limtrakul, J.; Illas, F.; Bromley, S. T. Magic Numbers in a One-Dimensional Nanosystem: ZnS Single-Walled Nanotubes. *J. Phys. Chem. C* **2013**, *117*, 22908–22914.

(39) Xu, W. Z.; Ye, Z. Z.; Ma, D. W.; Lu, H. M.; Zhu, L. P.; Zhao, B. H.; Yang, X. D.; Xu, Z. Y. Quasi-aligned ZnO Nanotubes Grown on Si Substrates. *Appl. Phys. Lett.* **2005**, *87*, 093110.